THE ASTROPHYSICAL JOURNAL, 458:L67–L70, 1996 February 20


# COUNTERROTATING STELLAR DISKS IN EARLY-TYPE SPIRALS: NGC 3593[1]

FRANCESCO BERTOLA, PIERANTONIO CINZANO, ENRICO MARIA CORSINI, AND ALESSANDRO PIZZELLA
Dipartimento di Astronomia, Università di Padova, vicolo dell'Osservatorio 5, I-35122 Padova, Italy

MASSIMO PERSIC
Osservatorio Astronomico, via G. B. Tiepolo 11, I-34131 Trieste, Italy and Scuola Internazionale Superiore di Studi Avanzati, Strada Costiera 11, I-34014 Trieste, Italy

AND

PAOLO SALUCCI
Scuola Internazionale Superiore di Studi Avanzati, Strada Costiera 11, I-34014 Trieste, Italy
*Received 1995 September 15; accepted 1995 December 8*

## ABSTRACT

We report the discovery of two counterrotating stellar disks in the early-type spiral galaxy NGC 3593.

The major axis kinematics shows the presence of two dynamically cold counterrotating components. The surface brightness profile is well reproduced by the sum of the contributions of two exponential disks of different scale lengths ($r_1 = 40''$; $r_2 = 10''$) and different central surface brightnesses ($\mu_{r,1} = 19.9$; $\mu_{r,2} = 18.5$ mag arcsec$^{-2}$). The $v$ and $\sigma$ radial profiles are easily reproduced by the means of a kinematical model adopting the above photometric parameters.

An ionized gas disk is present. It corotates with the smaller scale length and less massive ($M_2 = 2.7 \times 10^9\ M_\odot$) disk, and counterrotates with the larger and more massive ($M_1 = 1.2 \times 10^{10}\ M_\odot$) one.

We conclude that the smaller stellar disk is the result of a slow adiabatic acquisition of a conspicuous amount of counterrotating gas ($M_{\rm infall} \sim 4.3 \times 10^9\ M_\odot$) by the preexisting galaxy, originally constituted mainly by a gas-free stellar disk (disk 1). The counterrotating gas settled into the equatorial plane and then formed the inner stellar disk (disk 2).

*Subject headings:* galaxies: evolution — galaxies: formation — galaxies: individual (NGC 3593) — galaxies: kinematics and dynamics

## 1. INTRODUCTION

The phenomenon of counterrotation in disk galaxies has been so far reported to appear in three different types: (1) the overall counterrotation of the gaseous disk with respect to the stellar component found in several S0 galaxies (e.g., Galletta 1987; Bertola, Buson, & Zeilinger 1992) and in the early-type spiral NGC 3626 (Ciri, Bettoni, & Galleta 1995); (2) the counterrotation of the inner gas with respect to the outer gas, such as in the case of NGC 4826 (Braun, Walterbos, & Kennicutt 1992; Rubin 1994; Walterbos, Braun, & Kennicutt 1994); and (3) the counterrotation of two stellar disks with similar scale lengths and central surface brightnesses, such as in NGC 4550 (Rubin, Graham, & Kenney 1992; Rix et al. 1992), NGC 7217 (Merrifield & Kuijken 1994), and NGC 4138 (Broeils, Jore, & Haynes 1995).

In this Letter we report a new way of counterrotation in disk galaxies that extends case 3: in the Sa galaxy NGC 3593, two stellar exponential disks of different scale lengths and central surface brightnesses counterrotate. Furthermore, the gaseous disk counterrotates with respect to the higher scale length and more massive disk.

## 2. OBSERVATIONS AND RESULTS

The spectroscopic observations were made on 1994 February 18–19, using the Boller & Chivens spectrograph at the ESO 1.5 m spectroscopic telescope at La Silla. The No. 26 1200 groove mm$^{-1}$ grating, blazed at 5730 Å, was used in the first order in combination with a $2\farcs5 \times 4\farcm2$ slit. It yielded a wavelength coverage between 5200 and 7190 Å with a reciprocal dispersion of 64.8 Å mm$^{-1}$ and a spectral resolution of ~2.3 Å of FWHM. Every pixel on the No. 24 2048 × 2048 Ford CCD adopted as detector corresponded to 0.97 Å by $2\farcs43$ after on-chip binning.

Four spectra of NGC 3593 were taken, each with an exposure time of 3600 s. The nucleus of the galaxy was centered visually within the slit. The latter was aligned with the apparent major axis at a position angle of 92°. Comparison helium-argon lamp exposures were obtained after every object integration, and late G or early K giants were observed for templates with the same setup. The seeing during the observations was typically $1\farcs5$ FWHM during the two nights.

Using standard MIDAS routines all the spectra were bias-subtracted, flat-field–corrected by quartz lamp exposures, aligned removing tilts in the slit relative to the detector, and wavelength-calibrated by fitting the position of the comparison lines with cubic polynomials. The difference between the predicted theoretical wavelengths for night-sky OH and [O III] emissions (Osterbrock & Martel 1992), and those measured on each spectrum, corresponds to ~2 km s$^{-1}$ uncertainty due to wavelength calibration. Cosmic rays were found and corrected for by comparing the counts in each pixel with the local mean and standard deviation, and substituting a suitable value. The sky was determined from the edges of the galaxy frame resulting from the superposition of the four initial spectra, and then subtracted.

The gas velocities and velocity dispersions were measured by means of the MIDAS package ALICE. The position and

[1] Based on observations carried out at ESO, La Silla, Chile.

the FWHM of the [N II] lines ($\lambda_{rest}$ = 6548.0, 6583.4 Å), of the H$\alpha$ line ($\lambda_{rest}$ = 6562.8 Å), and of the [S II] lines ($\lambda_{rest}$ = 6716.5, 6730.8 Å) were determined by interactively fitting a Gaussian emission plus a polynomial continuum to each line and surrounding continuum. The center of the Gaussian was converted to velocity, and then the heliocentric correction was applied. The gas velocities derived from the different emission lines are in excellent mutual agreement; at each radius they have been averaged using $1/\sigma^2_{vel}$ (with $\sigma^2_{vel}$ expressed as a function of the relevant line signal-to-noise ratio [S/N]) as weighting factors. The variation of the rms velocity error $\sigma_{vel}$, as a function of S/N, was determined after fitting by quadratic polynomials the "velocity curve" of night-sky emission lines, whose S/N ratios had been previously measured.

The stellar velocity and velocity dispersion radial profiles were measured from the absorption lines in the wavelength range between about 5200 and 6200 Å, using the Fourier correlation quotient method (FCQ) (Bender 1990), as applied by Bender, Saglia, & Gerhard (1994). In deriving the above kinematical properties, the absorption line of Na at 5892.5 Å has been masked because of absorption contamination by the dust component. The spectrum was rebinned along the direction perpendicular to the dispersion in order to yield a minimum signal-to-noise ratio of 30.

NGC 3593 is member of the LGG 231 group, together with NGC 3623, NGC 3627, and NGC 3628 (Garcia 1993). It is classified as Sa(pec) by Sandage & Tammann (1987), and as S0/a(s): by de Vaucouleurs et al. (1991). It shows a chaotic pattern of dust patches throughout the face of the disk (Sandage & Bedke 1994). Its total $B$-band apparent magnitude is $B^0_T = 11.5$ mag (RC3), and the corresponding absolute luminosity is $L_B = 6 \times 10^9\ L_{B_\odot}$, for an assumed distance[2] of 12.4 Mpc (Rubin et al. 1985). The integrated spectral type of NGC 3593 is F5 (Humason, Mayall, & Sandage 1956).

The total masses of neutral and molecular hydrogen in NGC 3593 are $M_{H\,I} = 5.1 \times 10^8\ M_\odot$ and $M_{H_2} = 1.1 \times 10^9\ M_\odot$, respectively (Sage 1993).

The stellar rotation curve (Fig. 1) extends to about 60″ from the nucleus on either side, corresponding to about 4.3 kpc. In the region outward of 20″, the northwest side is receding while the southeast side is approaching. The contrary is true for the innermost region. We are therefore facing a case in which the inner stars are counterrotating with the outer ones. The velocity dispersion profile (Fig. 1) is characterized by a central minimum of 50 km s$^{-1}$. On both sides the velocity dispersion increases up to 120 km s$^{-1}$ at 15″, and then decreases outward down to about 60 km s$^{-1}$. At the same distance of stellar velocity dispersion maxima the equal strength of the two counterrotating components produces zero rotation velocity. The apparent asymmetries in the stellar kinematics are probably due to high-inclination dust absorption rather than being the signature of a dynamically young phenomenon.

In Figure 2 we present the stellar line-of-sight velocity distribution (LOSVD) obtained at different distances along the major-axis spectrum, using the FCQ package. The LOSVD profiles are clearly non-Gaussian outside the nucleus for $|r| < 30''$. At $r = 14''$ and $r = -18''$ a double peak is visible.

The strong emission lines present in NGC 3593 lead to a well-defined gas rotation curve (Fig. 1) extending to about 90″, corresponding to about 6.5 kpc, with $\Delta V = 240$ km s$^{-1}$. The gas

[2] We use $H_0 = 50$ km s$^{-1}$ Mpc$^{-1}$ throughout.

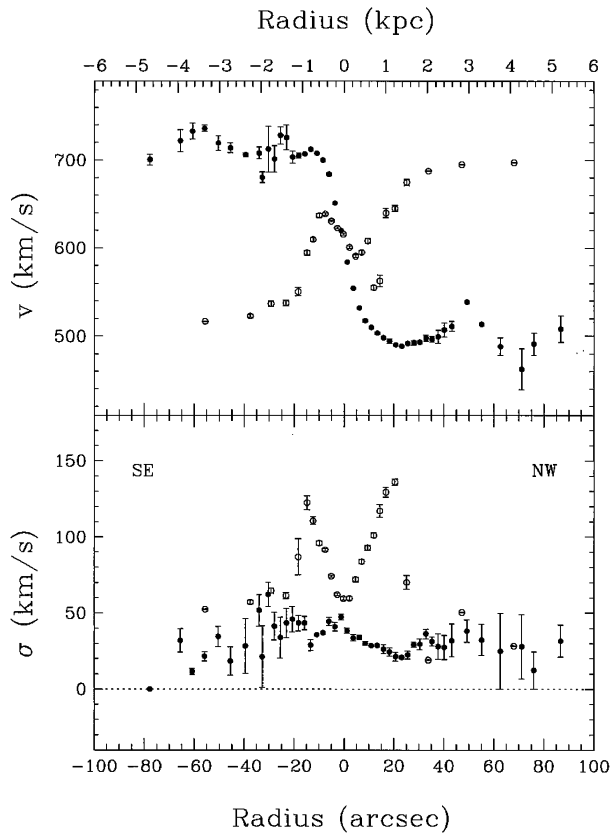


FIG. 1.—NGC 3593 major-axis kinematics: open circles denote measurements of the observed velocity and velocity dispersion radial profiles of the stellar component; filled circles denote measurements of the velocity and velocity dispersion of the ionized gas.

corotates with the inner stars and counterrotates with the outer ones. There is a good agreement between our gas rotation measurements and those of Rubin et al. (1985) in the region where they overlap ($r \leq 40''$). The gas velocity dispersion remains lower than 50 km s$^{-1}$. The line intensity profile for the five lines observed has two maxima, at about 9″ from the center on each side.

## 3. DISCUSSION

The photometric bulge/disk decomposition of NGC 3593 (Kent 1988) shows that the bulge-to-total light ratio is very low (B/T = 0.07), and that only in the innermost nuclear region ($r < 2''$) is the bulge contribution to the total surface brightness not negligible. Outside the bulge region, the Thuan-Gunn $r$-band surface brightness profile of NGC 3593 (Kent 1988) cannot be readily represented with a single exponential disk, owing to an abrupt change in slope at $r \sim 25''$: indeed, once subtracted the inner bulge from the total surface brightness, Kent (1988) interprets the residuals as due to a nonexponential disk (Fig. 3$a$). The more recent data of Ryder & Dopita (1994) are consistent with Kent (1988). In this Letter we proceed a step further: we keep Kent's bulge fixed, and interpret the nonexponential residuals as caused by the combination of two exponential disks, characterized respectively by scale lengths of $r_1 = 40''$ and $r_2 = 10''$, and by central surface brightnesses of $\mu_{r,1} = 19.9$ and $\mu_{r,2} = 18.5$ mag arcsec$^{-2}$ (see Fig. 3$a$). The corresponding integrated $B$-band luminosities of the two disks are $L_{B_1} = 4.9 \times 10^9\ L_{B_\odot}$ and $L_{B_2} = 1.1 \times 10^9\ L_{B_\odot}$

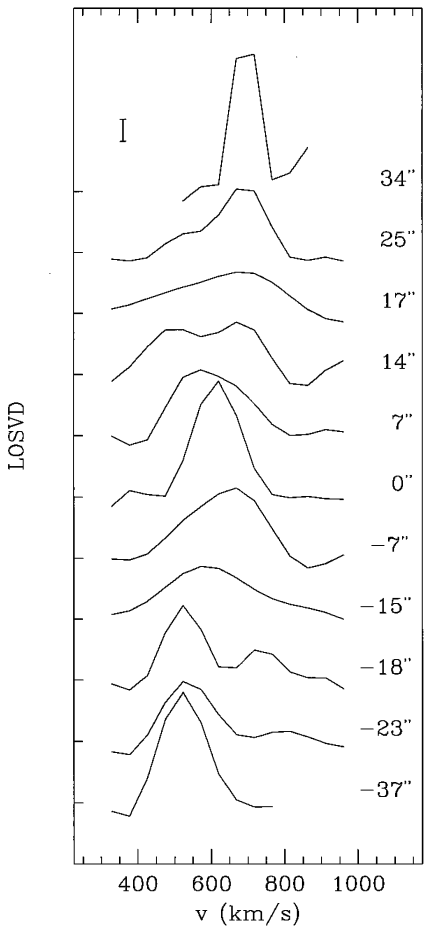


FIG. 2.—NGC 3593 major-axis line-of-sight velocity distribution (LOSVD), derived at various distances from the galaxy center. The different profiles have been vertically shifted and the ticks on the left represent the zero level. The LOSVD is proportional to the density of stars moving with velocity $v$. The $\pm 3\ \sigma$ error bar for an average signal-to-noise ratio is shown.

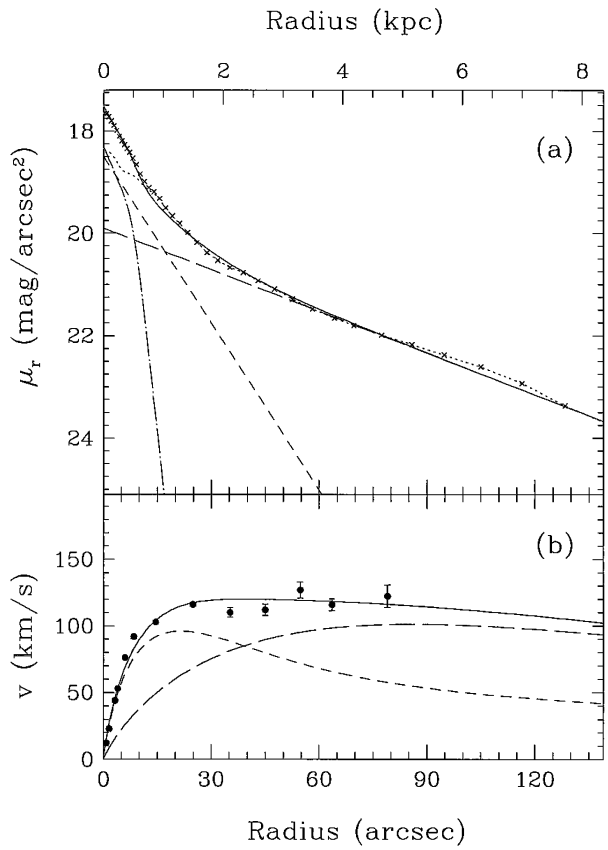


FIG. 3.—(*a*) Luminosity profile decomposition of NGC 3593. Kent (1988) decomposed the surface brightness along the major axis (*crosses*) into a bulge (*dot-dashed line*) and a nonexponential disk (*dotted line*). We decompose the latter into two disks: disk 1, with scale length $r_1 = 40''$ and central surface brightness $\mu_{r,1} = 19.9$ mag arcsec$^{-2}$ (*long-dashed line*), and disk 2, with $r_2 = 10''$ and $\mu_{r,2} = 18.5$ mag arcsec$^{-2}$ (*short-dashed line*). The sum of the three components, bulge, disk 1, and disk 2, is represented by the solid line. (*b*) Mass decomposition for NGC 3593. The dots represent the observed ionized gas velocity curve; the long-dashed line and short-dashed line represent the contribution of disk 1 and disk 2 to the total circular velocity (*solid line*), respectively. The contribution of the bulge is neglected.

(assuming the $B - r$ colors are the same for both disks). This photometric decomposition is supported by the mass decomposition. Indeed, the observed ionized gas rotation curve is well reproduced as the sum of the contributions of the two above exponential disks, neglecting the bulge contribution. The best fit to the ionized gas rotation curve is obtained with $M_1 = 1.2 \times 10^{10}\ M_\odot$ and $M_2 = 2.7 \times 10^9\ M_\odot$ (Fig. 3*b*). This result suggests that the two disks are characterized by similar $M/L$ ratios.

In the light of these photometric results, the interpretation of the stellar kinematics of NGC 3593 is straightforward. The observed stellar rotation curve and LOSVD are produced by the coexistence of two stellar disks, having the above-mentioned photometric properties, counterrotating with each other. As expected, the double absorption lines due to the two stellar disks are not detected throughout the spectrum, as in the case of NGC 4550 (Rubin et al. 1992; Rix et al. 1992), where the two disks are photometrically identical and give rise to X-shaped absorption lines: in fact, because of the different scale lengths and central surface brightnesses of the two disks in the inner and outer regions of NGC 3593, the spectrum is dominated by disk 2 and disk 1, respectively. The region where the two disks have approximately the same surface brightness falls at $r \sim 15''$ from the nucleus. Accordingly, the maxima in stellar velocity dispersion, falling exactly at this radius on either side of the center, are interpreted as caused by the double structure of the lines, as inferred from Figure 2. The low central stellar velocity dispersion ($\sigma_{\rm star} \approx 50$ km s$^{-1}$) is contributed by the low-luminosity bulge and the lower scale length disk.

In order to interpret the stellar kinematical behavior of NGC 3593, we calculated, for each point of the major axis, both the rotation velocity and the velocity dispersion for a model line profile; these were obtained assuming that each disk (1) is exponential, (2) has a Gaussian line profile, and (3) rotates with a spin vector opposite to that of the other disk, with the velocity that is obtained by approximate correction for the asymmetric drift of the circular velocity, inferred from the observed gas kinematics (assuming the gas is in circular orbits, as suggested by its low velocity dispersion, $\sigma_{\rm gas} < 50$ km s$^{-1}$). The assumption that each disk has a Gaussian line profile is motivated by the consideration that the overall shape of the observed line profile is determined mainly by differences in the kinematical properties of the two disks, rather than by the shapes of their individual line profiles. In order to better mimic

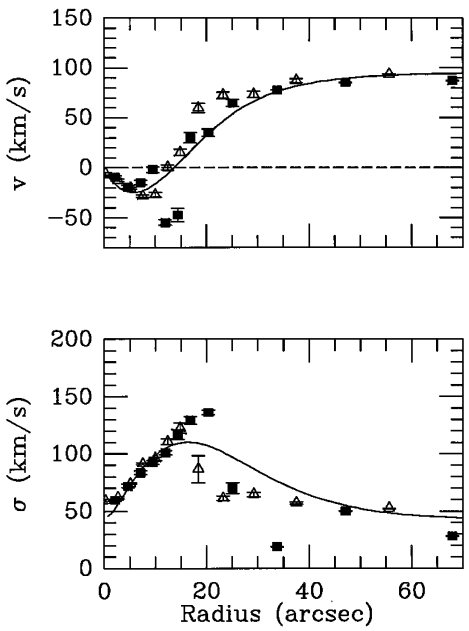


FIG. 4.—Observed stellar velocity and velocity dispersion radial profiles folded about the center (filled squares for the northwest side; open triangles for the southeast side), and the profiles expected (*solid line*) for the two-disk decomposition proposed (see text).

the response of the spectral analysis method (see, e.g., Cinzano & van der Marel 1994; Cinzano et al. 1995), the model line profile was analyzed by means of a Gaussian fit upon a Fourier space filtering that used the same wavenumber limits as in the analysis of the spectra. We did not take into account the effects of seeing, given that the Galactocentric distance of the region of interest to us is more than 4–5 times the seeing dispersion. In addition, given the simple approach of our modeling of the kinematics of NGC 3593, we have neglected the presence of the bulge, owing to its very modest size and light contribution.

In Figure 4 the observations of $v$ and $\sigma$ are compared with our model predictions. The satisfactory data-model agreement supports our proposed interpretation of NGC 3593 as being composed basically of (1) a small bulge, (2) a first, radially more extended, stellar disk that contains 80% of the total luminous mass and dominates the outer kinematics (disk 1), and (3) a second, radially more concentrated, stellar disk of lower total luminosity, which dominates the inner kinematics (disk 2). The angular momenta of the two disks are antiparallel. (From a purely kinematical point of view, the fit could be improved if disk 2 were truncated at 20″; this would lead to the steep drop in velocity dispersion and to the rapid rise in velocity. However, there is no obvious photometric evidence for a cutoff in disk 2 from Kent's data, so at present we regard this only as a possibility deserving further investigation.) The galaxy has also an H II disk corotating with disk 2.

Since H I, H II, $H_2$, and disk 2 counterrotate with respect to disk 1 (see Sage 1993 for H I and $H_2$ kinematics), the total counterrotating mass amounts to about 36% of disk 1.

Our data for NGC 3593, and our ensuing interpretation, can be explained if the smaller scale length disk has formed in a distinct process, as a result of the acquisition of a conspicuous amount of gas by the preexisting galaxy, originally constituted by a bulge and a stellar disk. The acquired disk has then formed stars. The fact that the two stellar disks of NGC 3593 are rather cold, as indicated by the velocity dispersion profile, could suggest that the gas has been acquired via slow infall (Ostriker & Binney 1991) into a galaxy characterized by a small bulge and a gas-free disk. The preexisting disk could remain unperturbed if the secondary (counterrotating) disk built up adiabatically. As Rix et al. (1992) suggest, for this scenario it is necessary that the primary disk was gas free, i.e., collisionless and, of course, that a significant gas supply was available for building the second disk. It is interesting, in this picture, that the gas (in different phases: ionized, neutral, and molecular) is also counterrotating with the primary disk, i.e., it belongs to the acquired baryonic mass and is a leftover from star formation in the secondary disk.

Smaller scale-length stellar disks which are the result of an acquisition, similar to the one described in this Letter but corotating with the preexisting disk, can be detected in two ways: first, looking at the luminosity profile, which should show the photometric signature of the presence of the disk, such as a change of slope in the cases where the inner disk emerges over the bulge (e.g., Rix & White 1990; Scorza & Bender 1990), and, second, looking at the absorption-line spectrum, because the interplay between the bulge and the inner disk can cause minimum velocity dispersion and maximum rotation velocity in the region where the inner disk prevails (e.g., Cinzano & van der Marel 1994).

We wish to thank M. Bernardi for her help in measuring the absorption lines using the FCQ package, kindly provided by R. Bender and R. Saglia. We are grateful to D. Burstein and H.-W. Rix for useful discussions and suggestions.

REFERENCES

Bender, R. 1990, A&A, 229, 441
Bender, R., Saglia, R. P., & Gerhard, O. E. 1994, MNRAS, 269, 785
Bertola, F., Buson, L. M., & Zeilinger, W. W. 1992, ApJ, 401, L79
Braun, R., Walterbos, R. A. M., & Kennicutt, R. C., Jr. 1992, Nature, 360, 442
Broeils, A. H., Jore, K. P., & Haynes, M. P. 1995, in preparation
Cinzano, P., Rix, H.-W., Zeilinger, W. W., & Bertola, F. 1995, MNRAS, submitted
Cinzano, P., & van der Marel, R. P. 1994, MNRAS, 270, 325
Ciri, R., Bettoni, D., & Galletta, G. 1995, Nature, 375, 661
de Vaucouleurs, G., de Vaucouleurs, A., Corwin, H. G., Jr., Buta, R. J., Paturel, G., & Fouquè, P. 1991, Third Reference Catalogue of Bright Galaxies (New York: Springer) (RC3)
Galletta, G. 1987, ApJ, 318, 531
Garcia, A. M. 1993, A&AS, 100, 47
Humason, M. L., Mayall, N. U., & Sandage, A. R. 1956, AJ, 61, 97
Kent, S. M. 1988, AJ, 96, 514
Merrifield, M. R., & Kuijken, K. 1994, ApJ, 432, 575
Osterbrock, D. E., & Martel, A. 1992, PASP, 104, 76
Ostriker, E., & Binney, J. 1989, MNRAS, 237, 785
Rix, H.-W., Franx, M., Fisher, D., & Illingworth, G. 1992, ApJ, 400, L5
Rix, H.-W., & White, S. D. M. 1990, ApJ, 362, 52
Rubin, V. C. 1994, AJ, 107, 173
Rubin, V. C., Burstein, D., Ford, W. K., Jr., & Thonnard, N. 1985, ApJ, 289, 81
Rubin, V. C., Graham, J. A., & Kenney, J. D. P. 1992, ApJ, 394, L9
Ryder, S. D., & Dopita, M. A. 1994, ApJ, 430, 142
Sage, L. J. 1993, A&A, 272, 123
Sandage, A., & Bedke, J. 1994, The Carnegie Atlas of Galaxies (Carnegie Inst. Washington Publ. 638)
Sandage, A., & Tammann, G. A. 1987, A Revised Shapley-Ames Catalog of Bright Galaxies (Carnegie Inst. Washington Publ. 635)
Scorza, C., & Bender, R. 1990, A&A, 235, 49
Walterbos, R. A. M., Braun, R., & Kennicutt, R. C., Jr. 1994, AJ, 107, 184